Ceramics International xxx (xxxx) xxx–xxx

Contents lists available at ScienceDirect

Ceramics International

journal homepage: www.elsevier.com/locate/ceramint

Effect of simultaneous K, and Yb substitution for Ca on the microstructural and thermoelectric characteristics of $CaMnO_3$ ceramics

A. Sotelo[a], M. Depriester[b], M.A. Torres[a], A.H. Sahraoui[b], M.A. Madre[a,*], J.C. Diez[a]

[a] Instituto de Ciencia de Materiales de Aragón (CSIC-Universidad de Zaragoza), Mª de Luna, 3, 50018 Zaragoza, Spain
[b] UDSMM (EA 4476), MREI-1, Université du Littoral Côte d'Opale, 59140 Dunkerque, France

ARTICLE INFO

Keywords:
Ceramics
Microstructure
Electrical properties
Thermal properties

ABSTRACT

$CaMnO_3$-based materials are very attractive among n-type thermoelectric oxides for high-temperature applications when they are appropriately doped. The main drawback of these materials is the cost associated to the necessary rare earth cations. This work aims decreasing the amount of these materials through a partial substitution of Ca^{2+} by an equimolar mixture of K^+ and Yb^{3+}, $Ca_{1-x}(K_{0.5}Yb_{0.5})_xMnO_3$, with x = 0.05, 0.10, 0.15, and 0.20. XRD studies have confirmed that the thermoelectric phase is the major one in all samples. Microstructure has shown the formation of large crystals, and an increasing porosity when the substitution is raised. This evolution has been confirmed through density measurements. Electrical resistivity has been drastically decreased for the 0.10 substituted samples, compared with the 0.05 ones, slightly increasing for higher substitution. On the other hand, absolute Seebeck coefficient and thermal conductivity are lower when the substitution is raised. The best ZT values have been achieved for the 0.10 substituted samples, which are around the typical reported in the literature for higher doping level. These results clearly point out to a decrease of the necessary rare earth dopant content to achieve similar performances in $CaMnO_3$ ceramics, which is of the main economic significance for their industrial production.

1. Introduction

Sustainability has to be based in energy economy, in which thermoelectric (TE) harvesting of wasted heat can play an important role due to its inherent operational simplicity, excellent scalability, and selfsustainability in remote or mobile applications [1]. As a consequence, they can raise the efficiency of classical energy transforming systems, decreasing their greenhouse gases emissions. In the last decades, most of the practical applications have been limited to classical semiconducting or intermetallic thermoelectric compounds due to their high performances [2], usually quantified through the dimensionless figure of merit, ZT ($=TS^2/\rho\kappa$, where T, S, ρ, and κ, are absolute temperature, Seebeck coefficient, electrical resistivity, and thermal conductivity, respectively) [3]. On the other hand, they possess some inconveniences, as they are composed of heavy and harmful elements with low abundance in the earth's crust, and their maximum working temperatures are relatively low.

These issues were avoided after the discovery of unexpected high thermoelectric properties in Na_xCoO_2 [4], composed of more abundant and environmentally friendly elements, together with its higher working temperature under air atmosphere, due to its ceramic nature. These advantages impelled the research in this field, finding new materials with both *p*- and *n*-type conduction. Among all these materials, it is possible to highlight the CoO- and MnO-based ones, respectively [5–8]. On the other hand, the main problem associated to these TE ceramics is their relative low performance, even at high temperatures. As a consequence, the main objective in the works related with these materials is centered in raising their performances through different routes. One of the most important is cation doping, which can be used to modify the charge carrier concentration, as well as provide defects to decrease thermal conductivity [7,9]. On the other hand, it is also possible to introduce defects in the structure without modification of charge carrier concentration through isovalent subtitutions. Moreover, the amount of defects can be raised, without modifying the charge carrier concentration, through aliovalent substitutions (as Dy^{3+}/Na^+ for Ca^{2+}) [9].

The objective of this work is producing high performance $CaMnO_3$ thermoelectric materials with simultaneous substitution of Ca by Yb, and K. They were added in the same atomic ratio in order to maintain constant the charge carrier concentration. Moreover, as K may be lost during the thermal treatment [10], the experimental conditions described in previous works [9] have been partially followed in order to

* Corresponding author.
E-mail address: amadre@unizar.es (M.A. Madre).

https://doi.org/10.1016/j.ceramint.2018.04.071
Received 22 March 2018; Received in revised form 9 April 2018; Accepted 9 April 2018

minimize K losses. The thermoelectric properties of the sintered bodies will be determined and related with their structural and microstructural features.

2. Experimental

The initial $Ca_{1-x}(K_{.5}Yb_{.5})_xMnO_3$ mixtures (x = 0.05, 0.10, 0.15, and 0.20) used in this work were prepared from commercial $CaCO_3$ (≥ 99%, Aldrich), Mn_2O_3 (99%, Aldrich), K_2CO_3 (PA, Panreac), and Yb_2O_3 (99.9%, Aldrich) powders. They were weighed in the appropriate proportions, mixed and milled 1 h at 300 rpm in a ball mill in distilled water media. After milling, the suspensions were dried using infrared radiation until all water has been evaporated. The powders were then cold uniaxially pressed at 400 MPa and subjected to a thermal treatment at 900 °C for 12 h in order to decompose the Ca, and K carbonates. The thermally treated bodies were subsequently manually milled, pressed at 400 MPa in form of pellets with the suitable dimensions for their characterization, and sintered in a closed alumina boat at 1300 °C for 12 h, with a final furnace cooling.

Phase identification in the sintered materials has been performed using powder X-ray diffraction (XRD) utilizing a Rigaku D/max-B X-ray powder diffractometer (CuKα radiation) with 2θ ranging between 10 and 70 degrees. Microstructural observations were performed on the samples surfaces using a Field Emission Scanning Electron Microscope (FESEM, Zeiss Merlin) fitted with an energy dispersive spectrometry (EDS) device. Apparent density was measured using Archimedes' principle in, at least, four samples for each composition, taking 4.705 g/cm^3 as the theoretical one [11].

Electrical resistivity and Seebeck coefficient were simultaneously determined in all samples using the steady state mode, by the standard dc four-probe technique in a LSR-3 apparatus (Linseis GmbH) between 50 and 800 °C. Thermal conductivity has been determined through the photothermal radiometry technique (PTR) at room temperature (RT). Here, a modulated laser beam (at 532 nm wavelength generated by a Ventus DPSS laser source internally modulated) is absorbed by the studied material standing on a thermally semi-infinite substrate. The light beam is beforehand enlarged by a telescopic arrangement to ensure a one-dimensional heat propagation inside the investigated system. Modulation frequency dependence of the temperature distribution is then a function of the thermal parameters of the material. In opaque samples and for small temperature variations, infrared total emittance radiated by the material is then directly proportional to its surface temperature [12]. This infrared radiation is then collected as a function of the modulation frequency with a Mercury Cadmium Tellurium (MCT) detector cooled at liquid nitrogen temperature (Teledyne Judson Technologies J15D12-M204-S01M-60). Output electric signal is then pre-amplified (Teledyne Judson Technologies PA 300) to be sent into a lock-in amplifier (EG&G 7260) for processing. Thermal parameters are extracted from the signal by the knowledge of the relationship linking the surface temperature with the thermal parameters using EG&G 7260 for processing [13].

ZT values were calculated at RT, using the power factor and thermal conductivity data. Moreover, as it is well known, $CaMnO_3$-based materials thermal conductivity decreases when temperature is raised [7], the ZT values have been estimated up to 800 °C, considering κ unchanged in the worst-case situation, and compared to the best up-to-date literature data.

3. Results and discussion

Powder XRD patterns of all samples are presented in Fig. 1. At a first sight it is clear that the highest peaks (identified by their diffraction planes) correspond to the thermoelectric phase [8,14]. Moreover, the $CaMn_2O_4$ phase can be also identified through the small intensity peaks (shown by *) [15]. When observing these small reflections, it is clear that their intensity is slightly raised when the substitution is increased.

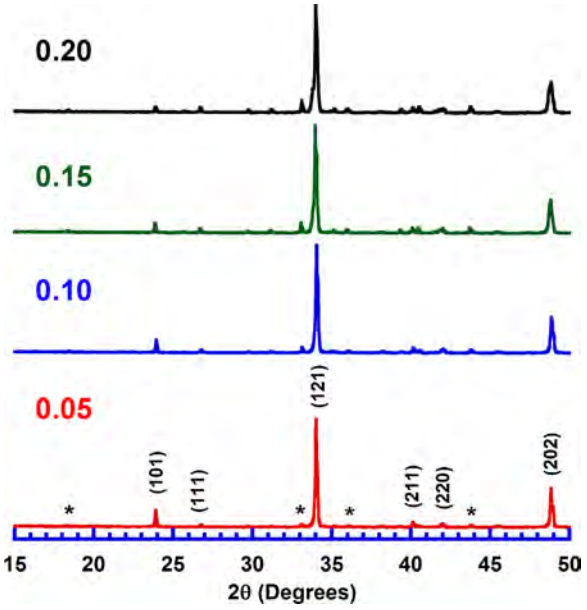

Fig. 1. Powder XRD patterns of $Ca_{1-x}(K_{0.5}Yb_{0.5})_xMnO_3$ samples for the different x values. Diffraction peaks indicate the thermoelectric phase, while * indicates the ones for $CaMn_2O_4$.

This behaviour indicates that Mn proportion in the sintered samples should be higher when the Yb, and K addition is raised. This result clearly points out to a possible total K_2CO_3 volatilization [10] and/or sublimation [16] in spite of the controlled conditions during the thermal treatments. This is an unexpected result when taking into account previous works which led to Dy, and Na co-doped $CaMnO_3$ with only partial Na losses [9].

FESEM observations on the surfaces of all samples are displayed in Fig. 2. As it can be observed in the micrographs, samples are composed of larger grains when the substitution is lower. Moreover, the raise in the Yb, and K content strongly increases the samples porosity. This effect could be due to the already mentioned K_2CO_3 losses during the sintering procedure, in agreement with the XRD data. EDS analysis performed in all samples has obtained only one phase, $Ca_{1-x}Yb_xMnO_3$, with Yb content very close to the nominal one. On the other hand, no $CaMn_2O_4$ phase has been identified in these samples, probably due to its low amount. Furthermore, no potassium has been found in any of the EDS analysis performed in the different samples, corroborating the previous considerations.

In order to confirm the porosity evolution previously observed in the samples, density values have been determined, and the results are summarized in Table 1. In spite of the large shrinkage observed in the samples after the sintering procedure, these data show a decrease of relative density when the substitution is raised, from around 89% for the lowest substitution, to about 72% for the highest one. Moreover, they are in agreement with the FESEM observations; and they are very repetitive, as can be deduced from the very low standard errors obtained in the measurements.

The microstructural evolution with the substitution is reflected in the electrical resistivity displayed in Fig. 3. As it can be observed in this graph, electrical resistivity decreases up to 0.10(Yb,K) added samples, slightly increasing for higher content. This behaviour can be explained taking into account several factors, as porosity, secondary phases content, and charge carrier concentration. As it is well known, electrical resistivity is increased when the porosity and secondary phases content is raised. On the other hand, due to the fact that K seems to be evaporated from the samples after sintering, electrical resistivity should be lower when the Yb content grows as it increases the charge carrier concentration (substitution of Ca^{2+} by Yb^{3+}). Consequently, the

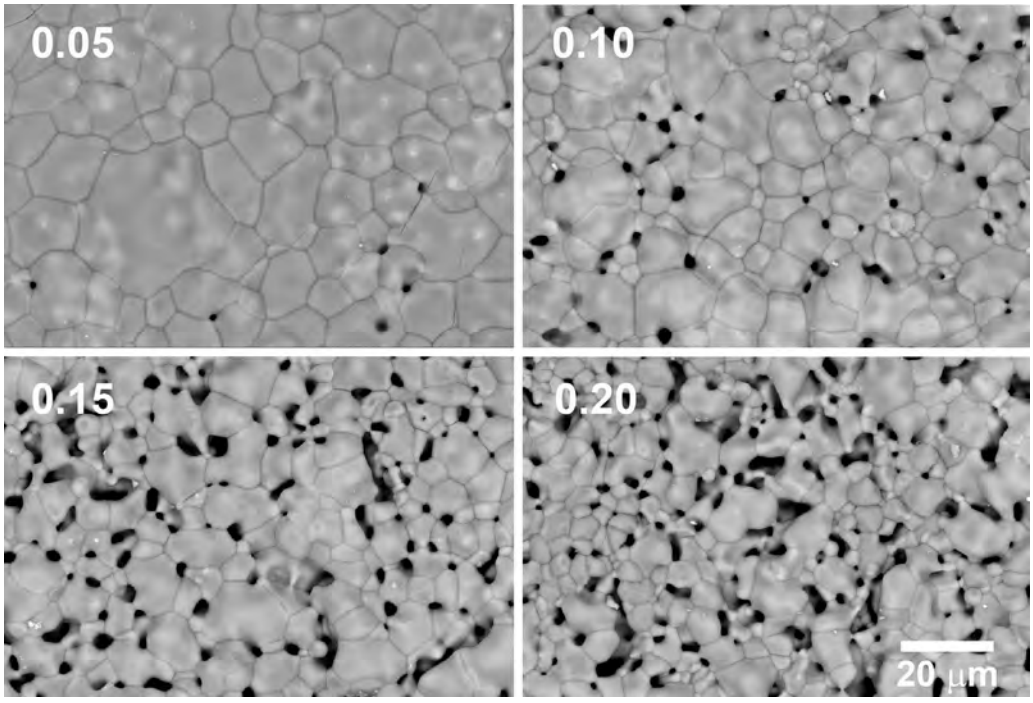

Fig. 2. FESEM micrographs performed in representative surfaces of $Ca_{1-x}(K_{.5}Yb_{.5})_xMnO_3$ sintered samples, with different x values.

Table 1
Mean density of $Ca_{1-x}(Yb_{.5}K_{.5})_xMnO_3$ samples, as a function of the Yb, and K addition, together with their standard errors, and the relative density taking the theoretical one as 4.705 g/cm^3 [11].

x	Density (g/cm^3)	Standard error	Relative density (%)
0.05	4.18	0.03	89
0.10	3.95	0.03	84
0.15	3.41	0.03	73
0.20	3.38	0.08	72

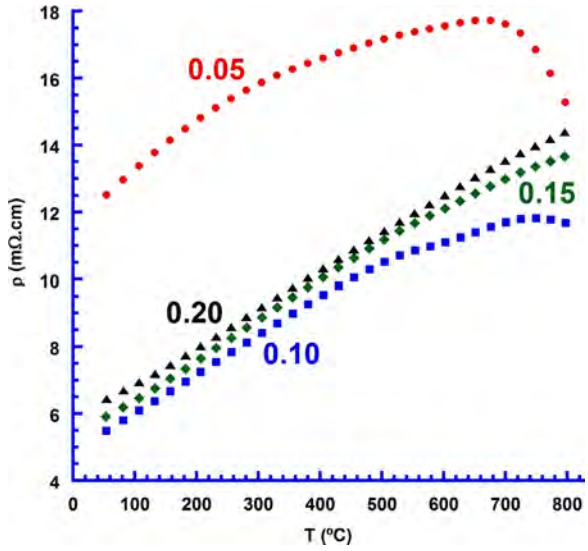

Fig. 3. Electrical resistivity evolution with temperature for $Ca_{1-x}(K_{0.5}Yb_{0.5})_xMnO_3$ sintered samples for the different x values.

decrease from the 0.05 to the 0.10 added samples can be associated to the higher influence of the raise of charge carrier concentration, with respect to the other factors. When the addition grows, the porosity and secondary phases have larger effect, leading to the slight increase in resistivity. Moreover, the general behaviour of resistivity is also modified by the substitution, with a drastic change in the 0.05 samples from metallic-like ($d\rho/dT > 0$) to semiconducting-like ($d\rho/dT < 0$) at around 650 °C, being softer for the 0.10 ones, and disappearing for higher substitution. The lowest values at room temperature have been determined in 0.10 samples (5.5 mΩ cm), which are much lower than the reported in undoped samples through sintering (125 mΩ cm) [17], or spark plasma sintering (SPS, 10 mΩ cm) [18]. Moreover, they are in the order of sintered Yb-doped $CaMnO_3$ (2.2–7 mΩ cm) [8,19–21].

When evaluating the samples at 800 °C, the minimum resistivity values measured in this work (11.5 mΩ cm) are much lower than the pristine $CaMnO_3$ (35 mΩ cm) [17]. On the other hand, they are higher than the obtained in undoped samples prepared through SPS (8 mΩ cm) [18], or in Yb-doped sintered materials (4–9 mΩ cm) [8,19–21]. These data clearly show that the K_2CO_3 loss during the sintering procedure is only affecting the high temperature electrical resistivity values, when compared to the Yb single doped materials.

Fig. 4 displays the variation of the Seebeck coefficient as a function of temperature for the different samples. All of them exhibit negative values in the whole measured temperature range, confirming an electron dominated conduction mechanism. Moreover, S behaviour is the same observed in the electrical resistivity, the absolute values are increased when the temperature is raised, except in the high temperature region (> 700 °C) where S decreases in the 0.05, and 0.10 samples. The highest absolute S values are measured in the 0.05 ones, in agreement with their higher electrical resistivity. At room temperature, the maximum values (−175 μV/K) are much lower than the reported in undoped materials (−350 μV/K) [17] which clearly reflects the typically low carrier concentration in $CaMnO_3$. The electron doping promoted by Yb substitution, due to the loss of K, enhances the carrier concentration and decreases Seebeck coefficient. On the other hand, these values are higher to the obtained in Yb-doped sintered samples (−90 to −100 μV/K) [8,19–21], prepared through SPS (−90 μV/K) [18], or in codoped materials (−70 to −120 μV/K) [22–24]. However, at 800 °C, the maximum values obtained in this work (−230 μV/K) are in the order of undoped samples (−225 μV/K) [17]. Moreover, they are much higher than the measured in Yb-doped (−140 to −160 μV/K) [8,19–21], or codoped $CaMnO_3$ sintered materials (−95 to −160 μV/K) [22–24].

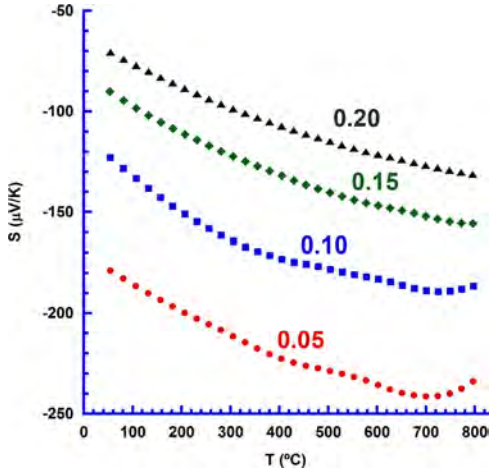

Fig. 4. Seebeck coefficient evolution with temperature for $Ca_{1-x}(K_{.5}Yb_{.5})_xMnO_3$ sintered samples for the different x values.

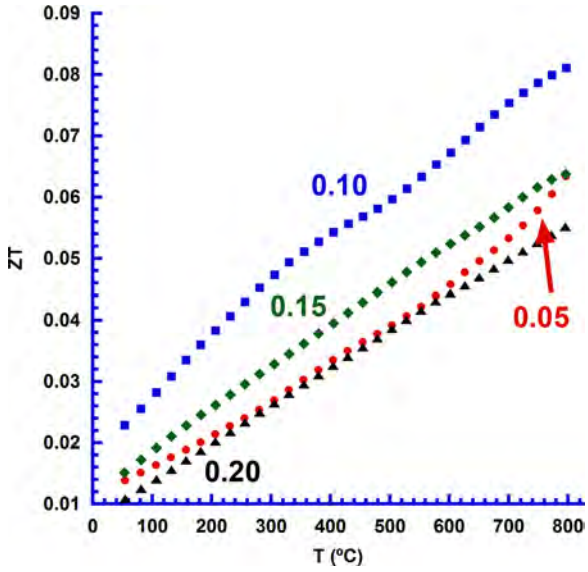

Fig. 5. ZT evolution with temperature for $Ca_{1-x}(K_{0.5}Yb_{0.5})_xMnO_3$ sintered samples for the different x values. Vertical dotted line divide the graph into calculated (low temperatures), and estimated (high temperatures) values considering κ unchanged with temperature.

Furthermore, they are still higher than the obtained in samples processed through SPS (−145 μV/K) [18].

Thermal conductivity at room temperature has been determined as 6.04, 3.93, 2.97, and 2.32 W/K m, for the 0.05, 0.10, 0.15, and 0.20 samples, respectively. The highest value is much higher than the measured in doped and codoped manganites (4.1–1.5 W/K m) [21,25,26] due to the high density of samples and the low dopant content. On the other hand, when the doping content is increased, density of samples decreased, lowering the thermal conductivities to be in the range of these reported values.

The evaluation of the samples thermoelectric performances has been performed through their ZT values. They have been calculated at room temperature using the electrical resistivity, Seebeck coefficient, and thermal conductivity. Moreover, they were estimated at higher temperatures using the room temperature thermal conductivity values. This assumption gives only underestimated values, as thermal conductivity typically decreases when the temperature is raised [21,25,26]. Consequently, the real high temperature ZT values should be higher than the presented in Fig. 5. As it can be observed in the graph, the maximum ZT values in the whole measured temperature range have been obtained in the 0.10 samples, corresponding to 0.05 rare earth doping, which is a lower amount than the reported for optimally doped $CaMnO_3$ materials [8,21,25]. Furthermore, the maximum values estimated in these samples at 800 °C (0.081) are around the obtained in more heavily doped ceramics (0.11–0.28) [21,25,26], taking into account their underestimation. Even if the thermoelectric performances obtained in this work are comparable to the reported in the literature, it is really important to highlight the lower content of rare earth cations in the samples produced in this work. This factor could be of the main economic significance when considering industrial production, due to the high costs, and low abundance in earth crust, of rare earth compounds.

4. Conclusions

$Ca_{1-x}(K_{0.5}Yb_{0.5})_xMnO_3$ (x = 0.05, 0.10, 0.15, and 0.20) polycrystalline samples have been successfully prepared through the classical solid state route. After sintering procedure, the samples have shown an important shrinkage, larger when the substitution was lower. Density measurements have demonstrated this evolution, with relative densities from 89% of the theoretical one for the 0.05 samples, to 72% for the 0.20 ones. XRD patterns showed that samples are mainly composed of the thermoelectric phase, while microstructure displays higher porosity content when the substitution is increased. All these features are reflected in the thermoelectric performances, reaching the minimum electrical resistivity for the 0.10 samples, which possess the best combination of density and dopant concentration. On the other hand, Seebeck coefficient and thermal conductivity are decreased when the substitution is raised, due to the higher Yb content and lower density, respectively. The maximum ZT at 800 °C has been estimated for the 0.10 samples, with similar values than the reported in the literature, but using much lower rare earth content. This is an important achievement, from an economic point of view and the relatively low abundance in the earth crust of rare earth raw materials, for their industrial production.

Acknowledgements

The authors wish to thank the Gobierno de Aragón-FEDER (Grupos de Investigacion Consolidados T12 and T87), MINECO-FEDER (MAT2017-82183-C3-1-R), and Universidad de Zaragoza (UZ2017-TEC-03) for financial support. Authors would like to acknowledge the use of Servicio General de Apoyo a la Investigación-SAI, Universidad de Zaragoza.

References

[1] M.H. Elsheikh, D.A. Shnawah, M.F.M. Sabri, S.B.M. Said, M.H. Hassan, M.B.A. Bashir, M. Mohamad, A review on thermoelectric renewable energy: principle parameters that affect their performance, Renew. Sustain. Energy Rev. 30 (2014) 337–355.

[2] H. Wang, J. Hwang, M.L. Snedaker, I.-H. Kim, C. Kang, J. Kim, G.D. Stucky, J. Bowers, W. Kim, High thermoelectric performance of a heterogeneous PbTe nanocomposite, Chem. Mater. 27 (2015) 944–949.

[3] D.M. Rowe, D.M. Rowe (Ed.), Thermoelectrics Handbook: Macro to Nano, 1st ed., CRC Press, Boca Raton, FL, 2006, pp. 1-3–1-7.

[4] I. Terasaki, Y. Sasago, K. Uchinokura, Large thermoelectric power in $NaCo_2O_4$ single crystals, Phys. Rev. B. 56 (1997) 12685–12687.

[5] A.C. Masset, C. Michel, A. Maignan, M. Hervieu, O. Toulemonde, F. Studer, B. Raveau, J. Hejtmanek, Misfit-layered cobaltite with an anisotropic giant magnetoresistance: $Ca_3Co_4O_9$, Phys. Rev. B. 62 (2000) 166–175.

[6] Sh Rasekh, G. Constantinescu, M.A. Torres, M.A. Madre, J.C. Diez, A. Sotelo, Growth rate effect on microstructure and thermoelectric properties of melt grown $Bi_2Ba_2Co_2O_x$ textured ceramics, Adv. Appl. Ceram. 111 (2012) 490–494.

[7] Y.H. Zhu, W.B. Su, J. Liu, Y.C. Zhou, J. Li, X. Zhang, Y. Du, C.L. Wang, Effects of Dy and Yb co-doping on thermoelectric properties of $CaMnO_3$ ceramics, Ceram. Int. 41 (2015) 1535–1539.

[8] A. Sotelo, M.A. Madre, M.A. Torres, J.C. Diez, Effect of synthesis process on the densification, microstructure, and electrical properties of $Ca_{0.9}Yb_{0.1}MnO_3$ ceramics, Int. J. Appl. Ceram. Technol. 14 (2017) 1190–1196.

[9] Y.C. Zhou, C.L. Wang, W.B. Su, J. Liu, H.C. Wang, J.C. Li, Y. Li, J.Z. Zhai, Y.C. Zhang, L.M. Mei, Electrical properties of Dy^{3+}/Na^{+} co-doped oxide thermoelectric $[Ca_{1-x}(Na_{1/2}Dy_{1/2})_x]MnO_3$ ceramics, J. Alloy. Compds 680 (2016) 129–132.
[10] A. Sotelo, F.M. Costa, N.M. Ferreira, A. Kovalevsky, M.C. Ferro, V.S. Amaral, J.S. Amaral, Sh Rasekh, M.A. Torres, M.A. Madre, J.C. Diez, Tailoring $Ca_3Co_4O_9$ microstructure and performances using a transient liquid phase sintering additive, J. Eur. Ceram. Soc. 36 (2016) 1025–1032.
[11] R. Lohnert, M. Stelter, J. Topfer, Evaluation of soft chemistry methods to synthesize Gd-doped $CaMnO_{3-\delta}$ with improved thermoelectric properties, Mater. Sci. Eng. B 223 (2017) 185–193.
[12] P.E. Nordal, S.O. Kanstad, Photothermal radiometry, Phys. Scr. 20 (1979) 659–662.
[13] M. Depriester, P. Hus, S. Delenclos, A.H. Sahraoui, New methodology for thermal parameter measurements in solids using photothermal radiometry, Rev. Sci. Instr. 76 (2005) 074902.
[14] F.-P. Zhang, Q.-M. Lu, X. Zhang, J.-X. Zhang, First principle investigation of electronic structure of $CaMnO_3$ thermoelectric compound oxide, J. Alloy. Compds. 509 (2011) 542–545.
[15] S. Zouari, L. Ranno, A. Cheikhrouhou, O. Isnard, M. Pernet, P. Wolfers, P. Strobel, New model for the magnetic structure of the marokite-type oxide $CaMn_2O_4$, J. Alloy. Compds. 353 (2003) 5–11.
[16] R.L. Lehman, J.S. Gentry, N.G. Glumac, Thermal stability of potassium carbonate near its melting point, Thermochim. Acta 316 (1998) 1–9.
[17] R. Kabir, R. Tian, T. Zhang, R. Donelson, T.T. Tan, S. Li, Role of Bi doping in thermoelectric properties of $CaMnO_3$, J. Alloy. Compds. 628 (2015) 347–351.
[18] S. Quetel-Weben, R. Retoux, J.G. Noudem, Thermoelectric $Ca_{0.9}Yb_{0.1}MnO_{3-\delta}$ grain growth controlled by spark plasma sintering, J. Eur. Ceram. Soc. 33 (2013) 1755–1762.
[19] D. Flahaut, T. Mihara, R. Funahashi, N. Nabeshima, K. Lee, H. Ohta, K. Koumoto, Thermoelectrical properties of A-site substituted $Ca_{1-x}Re_xMnO_3$ system, J. Appl. Phys. 100 (2006) 084911.
[20] Y. Wang, Y. Sui, J. Cheng, X. Wang, Z. Lu, W. Su, High temperature metal-insulator transition induced by rare-earth doping in perovskite $CaMnO_3$, J. Phys. Chem. C. 113 (2009) 12509–12516.
[21] R. Kabir, D. Wang, T. Zhang, R. Tian, R. Donelson, T.T. Tan, S. Li, Tunable thermoelectric properties of $Ca_{0.9}Yb_{0.1}MnO_3$ through controlling the particle size via ball mill processing, Ceram. Int. 40 (2014) 16701–16706.
[22] B. Zhang, A. Chang, Q. Zhao, H. Ye, Y. Wu, Synthesis and thermoelectric properties of Yb-doped $Ca_{0.9-x}Yb_xLa_{0.1}MnO_3$ ceramics, J. Electron. Mater. 43 (2014) 4048–4055.
[23] H. Wang, C. Wang, Synthesis of Dy doped $Yb_{0.1}Ca_{0.9}MnO_3$ ceramics with a high relative density and their thermoelectric properties, Mater. Res. Bull. 47 (2012) 2252–2256.
[24] Y. Zhu, C. Wang, H. Wang, W. Su, J. Liu, J. Li, Influence of Dy/Bi dual doping on thermoelectric performance of $CaMnO_3$ ceramics, Mater. Chem. Phys. 144 (2014) 385–389.
[25] J.W. Park, D.H. Kwak, S.H. Yoon, S.C. Choi, Thermoelectric properties of Bi, Nb co-substituted $CaMnO_3$ at high temperature, J. Alloy. Compds. 487 (2009) 550–555.
[26] Y.-H. Zhu, W.-B. Su, J. Liu, Y.-C. Zhou, J. Li, X. Zhang, Y. Du, C.-L. Wang, effects of Dy and Yb co-doping on thermoelectric properties of $CaMnO_3$ ceramics, Ceram. Int. 41 (2015) 1535–1539.